

Edge magnetization and local density of states in chiral nanoribbons

A. R. Carvalho, J. H. Warnes, and C. H. Lewenkopf

Instituto de Física, Universidade Federal Fluminense, 24210-346 Niterói, RJ, Brazil

(Dated: October 30, 2018)

We study the edge magnetization and the local density of states of chiral graphene nanoribbons using a π -orbital Hubbard model in the mean-field approximation. We show that the inclusion of a realistic next-nearest hopping term in the tight-binding Hamiltonian changes the graphene nanoribbons band structure significantly and affects its magnetic properties. We study the behavior of the edge magnetization upon departing from half filling as a function of the nanoribbon chirality and width. We find that the edge magnetization depends very weakly in the nanoribbon width, regardless of chirality as long as the ribbon is sufficiently wide. We compare our results to recent scanning tunneling microscopy experiments reporting signatures of magnetic ordering in chiral nanoribbons and provide an interpretation for the observed peaks in the local density of states, that does not depend on the antiferromagnetic interedge interaction.

PACS numbers: 73.22.Pr, 75.75.-c, 73.20.Hb

I. INTRODUCTION

Graphene shows a large variety of novel and unique electronic properties¹. Of particular interest is the emergence of magnetism in graphene nanostructures². The prediction of localized states at the edges of graphene nanostructures³, that are believed to give rise to edge magnetization⁴⁻⁶ with potential applications in spintronics,⁷ has attracted a lot of theoretical and experimental attention. Electronic structure calculations indicate that graphene nanoribbons (GNRs), depending on the crystallographic orientation of their edges, exhibit a ferromagnetic spin alignment along the edges and an antiferromagnetic interedge ordering^{4,7-10}. Several experiments report evidence of edge states¹¹⁻¹⁴, but direct observations of edge magnetization in graphene remains rather elusive.

The synthesis of GNRs was pioneered by lithographic patterning¹⁵⁻¹⁷. This technique produces rough edges, that give rise to short-range scattering, detrimental to the electronic mobility¹⁸ and to the formation of local magnetic moments¹⁹. More recently, by chemically unzipping carbon nanotubes, it became possible to obtain GNRs with very smooth edges²⁰⁻²². In general, the latter are chiral, that is, their edges do not follow neither the zigzag nor the armchair high-symmetry orientations. The local density of states (LDOS) of ultra-smooth edge chiral GNRs was recently investigated using scanning tunneling microscopy/scanning tunneling spectroscopy (STM/STS)¹⁴. The obtained STS spectra are the first direct experimental evidence of localized edge states in chiral GNRs. These results are the experimental motivation for this paper.

The theoretical studies of electronic properties of graphene nanoribbons with arbitrary edges date back to a pioneering paper in the field³. It has been established that, for sufficiently wide ribbons, there is always an enhancement of the density of states (DOS) due to dispersionless zero-energy edge states, except for GNRs with armchair terminations²³. In chiral GNRs, as in the

zigzag case, electron-electron interactions split the zero-energy bands and give rise to edge magnetization^{10,24}; whereas the Hubbard mean-field calculations¹⁰ indicate that local magnetization appears whenever the noninteracting DOS is enhanced¹⁰, density functional theory (DFT) calculations point to a sharp suppression of the edge magnetization for chiralities close to the armchair orientation²⁴.

In this paper, we investigate edge magnetization in graphene chiral nanoribbons. More specifically, we systematically study the local magnetization as a function of the GNRs chirality, width W , and doping, the latter cast in terms of a chemical potential μ . We use a Hubbard mean-field model and include a next-nearest-neighbor (nnn) hopping term t' in the tight-binding description. The latter is necessary to reproduce the low-energy DFT band structure calculations²⁵. We find that, for sufficiently large W , the local magnetization is a function of the chirality with a negligible dependence of W . The study of the GNRs edge magnetization M as a function of the chemical potential μ reveals a strong correlation between M and some characteristic features of the band structure. We compare our calculations of both the DOS and the DOS with recent (STS) experimental results recently obtained for chiral GNRs¹⁴. Our results indicate that, by using realistic values of t' in the tight-binding model, the simple interpretation reported in the literature^{10,14} of the experimentally observed peaks in STS spectra in terms of edge magnetic ordering is hardly justified. This conclusion calls for further experimental and theoretical investigations for evidence of magnetism in GNRs.

The paper is organized as follows. In Sec. II, we present the model Hamiltonian used in this study, introduce the notation to describe the geometry chiral edges, and review the theory. Our results are presented in Sec. III. We begin by analyzing the edge magnetization for zigzag GNRs, that serves as a guide for the discussion that follows. Next, in Sec. IIIB, we study the edge magnetization in chiral GNRs as a function of chiral angle, width

and doping. Finally, in Sec. III C, we show our results for the LDOS and discuss the connection between our findings and experimental results. We present our conclusions in Sec. IV.

II. THEORETICAL MODEL

A. Chiral nanoribbons: lattice parametrization

We define the primitive unit cells (PUCs) of a chiral GNR in terms of their widths and the crystallographic direction of their edges.²³ The GNR longitudinal orientation is characterized by the translation (or chiral) vector \mathbf{C}_h , see Fig. 1, defined as

$$\mathbf{C}_h = n\mathbf{a}_1 + m\mathbf{a}_2 \equiv (n, m), \quad (1)$$

where n and m are integers, whereas \mathbf{a}_1 and \mathbf{a}_2 are the lattice unit vectors. The length of the translation vector is $a = a_0\sqrt{m^2 + mn + n^2}$, where $a_0 \approx 0.246$ nm is the graphene lattice constant. For later convenience, we write \mathbf{C}_h in terms of its projection on the zigzag and armchair directions

$$\mathbf{C}_h = \mathbf{C}_{h,zz} + \mathbf{C}_{h,ac} = (n - m)\mathbf{a}_1 + m(\mathbf{a}_1 + \mathbf{a}_2). \quad (2)$$

In general, \mathbf{C}_h does not provide a precise characterization of the edges, since GNRs with the same translation vector can have a different number of edge atoms N_e and dangling bonds N_d per unit cell. The constraint that neither N_e nor N_d can be smaller than $m+n$,²³ is used to define ‘‘minimal edge’’ GNRs^{23,26} where $N_e = N_d = m+n$. In this case, \mathbf{C}_h describes the nanoribbon edges unambiguously. For the sake of simplicity, in this paper, we consider only minimal edge chiral GNRs.

The GNR orientation is also often specified by the chiral angle θ_c , defined as

$$\cos \theta_c = \frac{\mathbf{C}_h \cdot \mathbf{a}_1}{\|\mathbf{C}_h\| \|\mathbf{a}_1\|} = \frac{2n + m}{2\sqrt{n^2 + m^2 + nm}}. \quad (3)$$

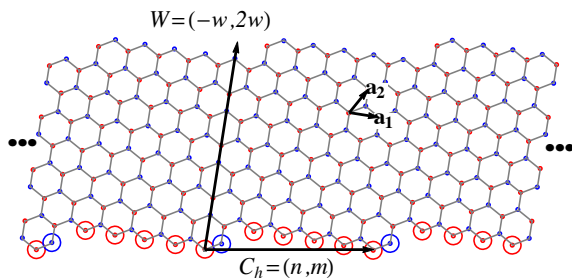


FIG. 1. (Color online) Representation of a chiral nanoribbon. The chiral vector is $\mathbf{C}_h = (5, 1)$, and the width is characterized by $\mathbf{W} = (-4, 8)$. The sites with dangling bonds at the GNR edges are indicated by circles.

Due to the symmetry of the honeycomb lattice, $0^\circ \leq \theta_c \leq 30^\circ$ accounts for all possible crystallographic direction. The high-symmetry cases are those where the GNR edges correspond to the zigzag and armchair directions, that is, $\theta_c = 0^\circ$ with a translation vector $(n, 0)$ and $\theta_c = 30^\circ$ with (n, n) , respectively. GNRs, whose edges are neither armchair nor zigzag, are called chiral.

The GNR width is conveniently characterized by¹⁰

$$\mathbf{W} = -w\mathbf{a}_1 + 2w\mathbf{a}_2 \equiv (-w, 2w), \quad (4)$$

where w is an integer. The vector \mathbf{W} is parallel to the armchair lattice orientation, see Fig. 1. The width of the chiral (and zigzag) GNRs is $W = \sqrt{3}wa_0 \cos \theta_c$.

B. Model Hamiltonian: Electronic structure

The ground-state magnetic ordering driven by electron-electron interaction has been extensively studied for GNRs with zigzag edges by a number of methods²⁵. Band structures calculated by density functional theory with local spin-density approximation (DFT-LSDA)^{7,27} show remarkable agreement with those obtained from a tight-binding model with a Hubbard term in the mean-field approximation²⁸. Further studies treating the e - e interaction beyond mean-field, such as Hartree-Fock with configuration interactions^{29,30} and quantum Monte Carlo³¹⁻³³, confirm that the mean-field approximation provides a good description of the magnetic ground-state properties of zigzag GNRs.

In this study, we use the Hubbard mean-field approximation to compute the electronic and magnetic properties of GNRs. As discussed, this simple model leads to results that agree with more sophisticated methods. Moreover, it allows for assessing the ground-states properties of GNRs with large primitive unit cells at a very modest computational cost. The model Hamiltonian reads

$$H = -t \sum_{\langle i,j \rangle, \sigma} \left(a_{i,\sigma}^\dagger a_{j,\sigma} + \text{H.c.} \right) - t' \sum_{\langle\langle i,j \rangle\rangle, \sigma} \left(a_{i,\sigma}^\dagger a_{j,\sigma} + \text{H.c.} \right) + U \sum_{i,\sigma} n_{i,\sigma} \langle n_{i,-\sigma} \rangle, \quad (5)$$

where $a_{i,\sigma}^\dagger$ and $a_{i,\sigma}$, respectively, are the creation and annihilation operators of electrons with spin projection σ at site i , while $n_{i,\sigma} = a_{i,\sigma}^\dagger a_{i,\sigma}$ is the number operator and $\langle n_{i,\sigma} \rangle$ is its expectation value. The symbols $\langle \dots \rangle$ and $\langle\langle \dots \rangle\rangle$ indicate that the sums run over nearest-neighbor and next-nearest-neighbor lattice sites, respectively.

The magnitude of the on-site Coulomb energy U in graphene systems is under current debate in the literature³⁴. At the tight-binding level, several authors study parametrizations containing higher nearest neighbor contributions (see, for instance, Ref. 35) and their effect on breaking the particle-hole symmetry. We take the pragmatic approach of taking the model parameters t , t' , and U that reproduce with great accuracy the low-energy

band structure and the local magnetization obtained by DFT-LSDA calculations for narrow nanoribbons²⁸. In our study, we do not consider edge reconstructions³⁶ and assume that the dangling bonds of undercoordinated edge atoms are passivated by hydrogen atoms, that have a similar electronegativity to the carbon ones.

We use the system translational invariance to write the eigenvalue problem in k -space. This is conveniently performed by means of the transformation

$$b_{kl,\sigma} = \frac{1}{\sqrt{M}} \sum_m e^{imka} a_{ml,\sigma} \quad (6)$$

where k is the wave number and a is the length of the translation vector. The sites are labeled $i = (m, l)$, where l denotes the lattice site within the GNR primitive unit cell and m labels the PUCs.

The Hamiltonian Eq. (5) now reads

$$H_k = \sum_{l'l,\sigma} H_{l'l,k\sigma} b_{kl,\sigma}^\dagger b_{k'l',\sigma}, \quad (7)$$

with matrix elements

$$H_{l'l,k\sigma} = -\tilde{t}_{l'l,k} + U\delta_{l'l}\langle n_{l,-\sigma} \rangle \quad (8)$$

that are independent of m due to translational invariance, namely, $\langle n_{i\sigma} \rangle \equiv \langle n_{ml,\sigma} \rangle = \langle n_{l\sigma} \rangle$. For sites within the same PUC, $\tilde{t}_{l'l,k}$ represents the nearest and the next-nearest hopping integrals t and t' . For neighboring sites at different PUCs, the hopping terms acquire the phase $e^{\pm ika}$.

The occupations $\langle n_{l,\sigma} \rangle$ are obtained self-consistently. The problem is defined with the help of the eigenenergies $\{\varepsilon_{k\nu,\sigma}\}$ and eigenfunctions $\{\varphi_{k\nu,\sigma}(l)\}$ of $H_{l'l,k\sigma}$: For a given wave number k , the ν th state occupation follows the Fermi distribution at zero temperature, namely, $\langle n_{k\nu,\sigma} \rangle = \Theta(\mu - \varepsilon_{k\nu,\sigma})$, where Θ is the Heaviside step function and μ is the chemical potential. The probability amplitudes $\varphi_{k\nu,\sigma}(l)$ allow one to calculate the l -site occupation for a fixed k using

$$\langle n_{kl,\sigma} \rangle = \sum_\nu |\varphi_{k\nu,\sigma}(l)|^2 \langle n_{k\nu,\sigma} \rangle. \quad (9)$$

Finally, the occupation appearing in Eq. (8) is obtained by integrating $\langle n_{kl,\sigma} \rangle$ over the Brillouin zone, namely,

$$\langle n_{l,\sigma} \rangle = \int \frac{dk}{\mathcal{V}_{\text{BZ}}} \langle n_{kl,\sigma} \rangle = \frac{1}{M} \sum_k \langle n_{kl,\sigma} \rangle, \quad (10)$$

where \mathcal{V}_{BZ} is the ‘‘volume’’ of the Brillouin zone.

The ground-state energy per unit cell E_0 is a sum of the occupied self-consistent single-particle state energies minus a standard term accounting for double counting the on-site Coulomb interaction energy, namely,

$$E_0 = \sum_{\nu,\sigma} \int \frac{dk}{\mathcal{V}_{\text{BZ}}} \langle n_{k\nu,\sigma} \rangle \varepsilon_{k\nu,\sigma} - \frac{U}{2} \sum_{l,\sigma} \langle n_{l,\sigma} \rangle \langle n_{l,-\sigma} \rangle. \quad (11)$$

The l th-site magnetization (in units of $\mu_B/2$) is defined as

$$M_l = \langle n_{l,\uparrow} \rangle - \langle n_{l,\downarrow} \rangle. \quad (12)$$

For chiral nanoribbons, one is frequently interested in the average edge magnetization, conveniently defined as

$$M = \frac{a_0}{a} \sum_{l \in \text{edge}} M_l, \quad (13)$$

where a is the length of the chiral translation vector and the sum runs over the sites of the sublattice (A or B) with the largest number of dangling bonds along the chiral GNR edge, see Fig. 1.

The LDOS reads

$$\rho_\sigma(\varepsilon, l) = \sum_\nu \int \frac{dk}{\mathcal{V}_{\text{BZ}}} |\varphi_{k\nu,\sigma}(l)|^2 \delta_\Gamma(\varepsilon - \varepsilon_{k\nu,\sigma}), \quad (14)$$

where δ_Γ is the Dirac δ -function broadened over an energy range Γ , taken to be much smaller than the typical energy separation between bands. In turn, the density of states is given by $\text{DOS}(\varepsilon) = \sum_{l,\sigma} \rho_\sigma(\varepsilon, l)$.

III. RESULTS

A. Nanoribbons with zigzag edges

We begin by presenting the band structure and magnetic properties of zigzag GNRs. Part of this material can be found in the literature (see, for instance, Refs. 2 and 25 for a review), but the analysis we present serves as an important guide for the subsequent discussion of the chiral GNRs results.

For $U = 0$ and $t' = 0$, the dispersionless edge modes enhance dramatically the LDOS at the GNR charge neutrality point³. When $U \neq 0$, due to the Stoner mechanism, the large LDOS at the GNR edges give rise to a local magnetization, and the electronic band structure shows a gap around $\varepsilon = 0$ for $\mu = 0$ ³. See Fig. 2a. The ground state shows a parallel spin alignment along each edge and antiferromagnetic interedge order. This is consistent with Lieb’s theorem³⁷, which asserts that the ground state of the Hubbard model of a bipartite lattice with nearest-neighbor hopping has spin $S = 0$.

Ab initio calculations of zigzag GNR band structures do not show particle-hole symmetry^{7,27}. The Hamiltonian (5) successfully reproduces the DFT band structure dispersion relations in the vicinity of the charge neutrality point at the expense of taking $t' \neq 0$ ²⁸. In this case, Lieb’s theorem³⁷ is no longer applicable and the natural question to ask is how robust is the ground state antiferromagnetic phase.

This issue is partially understood by a closer analysis of the localized edge states as a function of k . For $U = 0$, the lowest energy $|\varepsilon|$ modes become dispersionless at $k \gtrsim 2\pi/3a$, see Fig. 2(a). As k increases the states

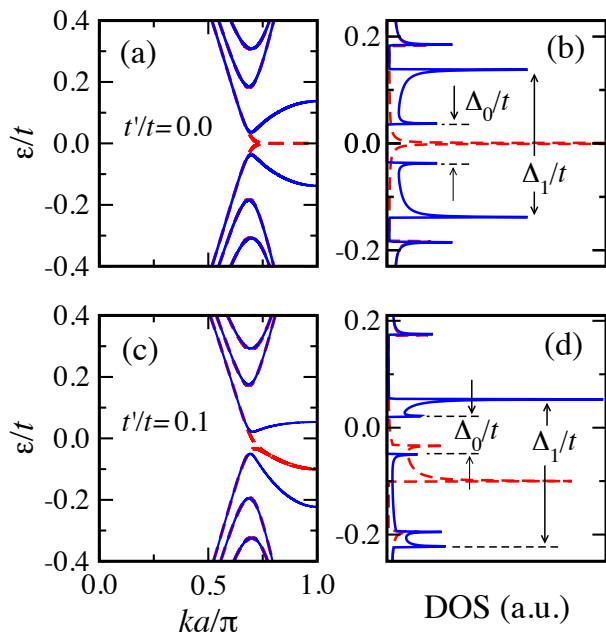


FIG. 2. (Color online) Band structure (left column) and corresponding density of states (right column) of a zigzag graphene nanoribbon of $N = 24$ for $t'/t = 0$ (upper row) and $t'/t = 0.1$ (lower row). The solid lines stand for the case of $U/t = 1$, while the dashed ones stand for $U = 0$.

become increasingly localized at the GNR edges. This behavior persists when $U \neq 0$. Accordingly, one spots two characteristic gaps in the GNR dispersion relations, see Fig. 2. The band gap Δ_0 occurs at the vicinity of the edge localization transition. The gap Δ_1 at $k = \pi/a$ is more relevant to the analysis of the system magnetic properties. The $k = \pi/a$ point corresponds to the most localized states along the GNR edges, which dominate the Stoner magnetization criterion.

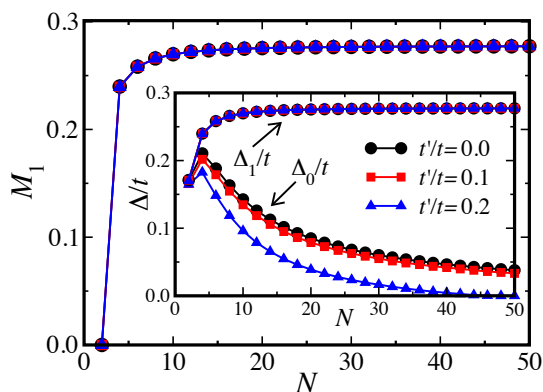


FIG. 3. (Color online) Edge magnetization M_1 of zigzag graphene nanoribbons as a function of their width N . Inset: Band gaps Δ_0 and Δ_1 versus N . In both cases $U/t = 1.0$ and $t'/t = 0.0, 0.1, \text{ and } 0.2$.

Based on this argument, one expects Δ_1 and the edge magnetization M_1 to be related. This is indeed observed in Fig. 3, that shows Δ_0 , Δ_1 , and M_1 as a function of the zigzag GNR width, here conveniently expressed in terms of N as the number of zigzag chains crossing the ribbon transversal direction, namely, $W = (\sqrt{3}N/2 + 1/\sqrt{3})a_0$. While Δ_0 decreases with increasing GNR width, Δ_1 and M_1 show a weak N dependence. We stress that neither Δ_1 nor M_1 show a significant dependence on t' .

Before proceeding, it is worth noticing that Figs. 2(b) and 2(d) anticipate some important features we discuss in the analysis of the STS spectra of chiral GNRs. While in the particle-hole symmetric case ($t' = 0$), the lowest energy $|\varepsilon|$ peaks in the density of states can be clearly associated with spin-polarized states, this is not true for $t' \neq 0$. In Fig. 2(d), the peak at $\varepsilon/t \approx -0.19$ corresponds to the van Hove singularity of a band unaffected by turning on the interaction U , while the peak at $\varepsilon/t \approx -0.22$ is the one related to a magnetic state.

Let us now study the behavior of the edge magnetization M_1 away from the charge neutrality point, or more precisely, as a function of the chemical potential $|\mu|$. One expects that, for μ values close to $\Delta_1/2$, states with opposite spin orientation with respect to the ground state start to be occupied and the edge magnetization to be suppressed. This is nicely illustrated in Fig. 4, that shows that M_1 vanishes for $|\mu| \gtrsim \Delta_1/2$. Our calculations also indicate that Δ_1 slowly decreases with increasing doping (not shown).

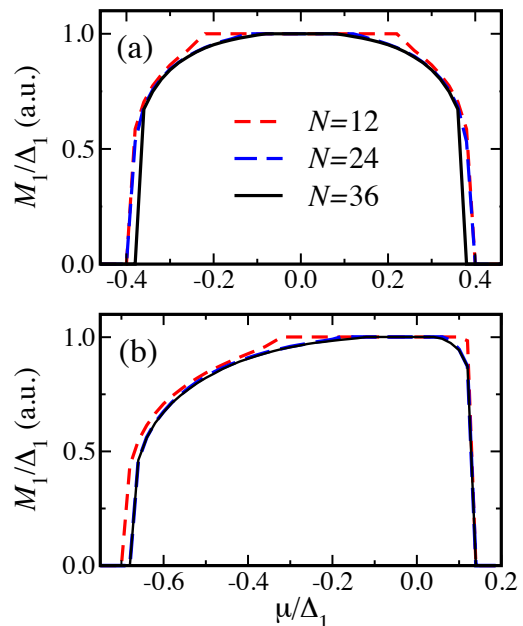


FIG. 4. (Color online) Edge magnetization M_1 as a function of the chemical potential μ for zigzag nanoribbons with different GNR widths N for (a) $t'/t = 0.0$ and (b) $t'/t = 0.1$. In both cases $U/t = 1$.

Figure 4 shows that the edge magnetization M_1 scaled by Δ_1 as a function of the chemical potential μ shows a

universal-like behavior for $N \gg 1$. For $t' = 0$, M_1/Δ_1 is an even function of μ/Δ_1 . For very narrow GNRs ($N \lesssim 20$), M_1/Δ_1 versus μ shows a maximum value, corresponding to a plateau of a width on the order of μ/Δ_0 . With increasing width, Δ_0 decreases and so does the plateau width. Figure 4(a) shows that, already for $N \gtrsim 30$, the edge magnetization no longer depends on N . The results are qualitatively similar for the more realistic case of $t' \neq 0$ ²⁸ as illustrated by Fig. 4(b).

A lot of attention has been devoted to the study of the competition between the anti- and the ferromagnetic phases in GNRs^{38,39}. Within the Hubbard mean field (for $t' = 0$) approximation, Jung and collaborators⁹ studied the antiferromagnetic interedge superexchange interaction to estimate the energy difference $\Delta E = E_0^{\text{FM}} - E_0^{\text{AFM}}$ between the antiferromagnetic ground state and the energetically lowest ferromagnetic configuration. A good fit to numerical calculations is

$$\Delta E/t = \frac{\alpha}{N^2 + C} \quad (15)$$

where $\alpha = 0.245$ and $C = 38.9$ for $t' = 0$, while $\alpha = 0.198$ and $C = 45.9$ for $t'/t = 0.1$. These values are smaller than the values reported in Ref. 8 but are in line with those of Ref. 9 for $t' = 0$ and $U = 2.0$ eV. Note, that ΔE becomes comparable with $k_B T$ at room temperature for $N \gtrsim 10$. Hence, for most experimental GNR samples currently available, where $N \gg 1$, the interedge interaction is quite negligible.

For doped systems, Lieb's theorem³⁷ does not apply, and ground-state phases, other than the antiferromagnetic phases are allowed. Some authors^{38,39} find a very rich phase diagram for zigzag GNRs of $10 \leq N \leq 30$. We have not performed a systematic investigation of non-collinear ground-state solutions as a function of μ since this issue is not central to the goals of our investigation. However, it is worth mentioning that, for all tested initial configurations (other than the anti- and the ferromagnetic ones), our self-consistent calculations give antiferromagnetic ground states for $|\mu| \lesssim \Delta_1/2$. This is an indication that a detailed determination of the magnetic phases can be quite daunting and beyond the scope of the model Hamiltonian we use.

What is the ground state configuration for $t' \neq 0$? In this case, the ferromagnetic ground state at half-filling is no longer forbidden by Lieb's theorem. However, for realistic values of t'/t ²⁸, our calculations only lead to (interedge) antiferromagnetic ground states at the charge neutrality point, but we find other phases very close in energy. We conclude that, except for very narrow bottom-up grown GNRs, the experimental assessment of this phase diagram is very daunting. For this reason, we focus our study on the spin alignment along a single edge.

B. Magnetization in GNR with chiral edges

As discussed above, for zigzag GNRs, the next-nearest-neighbor hopping term modifies and reduces the edge

LDOS at the charge neutrality point, but surprisingly it does not change the magnitude of edge magnetization. Is the scenario the same for chiral GNRs and how robust is the edge magnetization in this case? These are the issues we address in this section.

In the absence of electron-electron interaction, the nearest-neighbor tight-binding model shows an enhanced DOS at $\varepsilon = 0$ due to a dispersionless band corresponding to edge states. Using a continuous rotation of the graphene band structure, it was shown²³ that, in the infinite-width limit,

$$\rho_0(\theta_c) = \frac{2}{3a_0} \cos\left(\theta_c + \frac{\pi}{3}\right), \quad (16)$$

where ρ_0 is the average edge density of states at $\varepsilon = 0$. It is largest for zigzag nanoribbons and vanishes for the armchair ones. For chiral GNRs, $0 < \theta_c < 30^\circ$, ρ_0 shows a nearly linear dependence on θ_c . As discussed previously, the large enhancement of ρ_0 at the charge neutrality point is key for explaining the edge magnetization in GNRs in terms of the Stoner mechanism. As discussed in Ref. 10, although the edge magnetization M is proportional to ρ_0 , the band gap Δ_0 (for $t' = 0$) is related to U/t .

The degeneracy of the zero-energy dispersionless modes (for $U = 0$) can be understood in terms a band folding scheme put forward in Ref. 26: One can use Eq. (2) to write the chiral vector in terms of zigzag and armchair projections, namely, $\mathbf{C}_h = \mathbf{C}_{h,\text{zz}} + \mathbf{C}_{h,\text{ac}} = (n - m)\mathbf{a}_1 + m(\mathbf{a}_1 + \mathbf{a}_2)$. Since the armchair component does not lead to edge states, minimal edge (n, m) GNRs show a spectrum similar to the $(n - m, 0)$ zigzag ones close to $\varepsilon = 0$. By repeatedly folding the bands of the zigzag edge GNR $(1, 0)$, one finds the band structure of a $(S, 0)$ edge ribbon. S is conveniently written as $S = I + 3P$, where $I = 1, 2, 3$ and $P = 0, 1, 2, \dots$. For $I = 1$ and 2 , the spectrum has a Dirac-like point at $k \approx 2\pi/3$, while for $I = 3$, the Dirac point moves to $k = 0$. For $S \geq 3$, the zero-energy states extend over the whole Brillouin zone. The degeneracies of the zero-energy states are either $2P$ or $2(P + 1)$ depending on I as illustrated in Fig. 2 of Ref. 26. It is simple to show that, in the limit of $S \gg 1$, the folding rule leads to the ρ_0 given by Eq. (16).

In Fig. 5, we show the band structures obtained using the model Hamiltonian of Eq. (5) for the chiralities (a) $(2, 1)$ with $\theta_c = 19.1^\circ$ and (b) $(3, 1)$ with $\theta_c = 13.9^\circ$. Here, we take $U/t = 1$ and consider the cases of $t' = 0$ and $t'/t = 0.1$, both at half-filling. As before, $t' \neq 0$ breaks the particle-hole symmetry. As a result, the band gap Δ_0 goes to zero in most cases, even for very narrow nanoribbons. In distinction to the zigzag case, the k point corresponding the maximally localized states at the edges depends on the chirality, namely, $ka = \pi$ [Fig. 5(a)] for the chirality $(2, 1)$ and $k = 0$ [Fig. 5(c)] for $(3, 1)$.

Accordingly, we define Δ_1 as the energy gap around $\varepsilon \approx 0$ calculated at the $k = \pi/a$ point, corresponding to maximally localized edge states. Figure 6 shows Δ_1 as a function of the GNR width w for chiralities $(3, 1)$

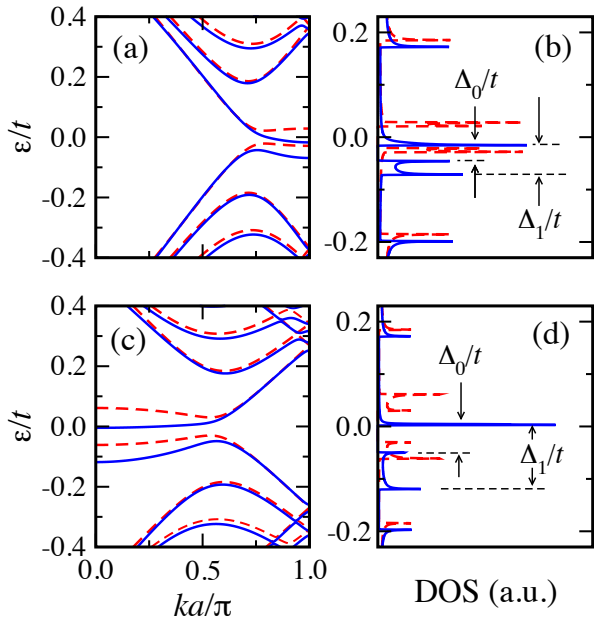


FIG. 5. (Color online) Electronic band structure for GNRs of width $w = 12$ and $U/t = 1$, with chiralities (a) (2,1) and (c) (3,1). Corresponding density of states for the (b) (2,1) and (d) (3,1) chiralities. The solid lines stand for the case of $t'/t = 0.1$, while the dashed ones stand for $t'/t = 0.0$. The energy gaps Δ_0 and Δ_1 are only indicated for the $t'/t = 0.1$ case.

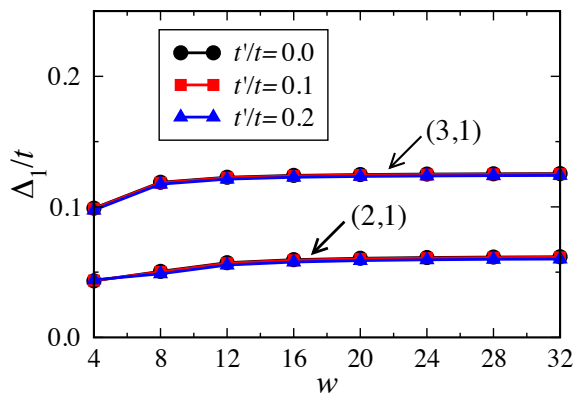


FIG. 6. (Color online) Gap Δ_1 as a function of the GNR width w for different next-nearest-neighbor hopping parameters t'/t . Here, we use $U/t = 1.0$.

and (2,1). We find that Δ_1 is independent of t' within the parameter range of that fits the DFT calculations.²⁸ Hence, the numerical results indicate that $t' \neq 0$ does not significantly change the edge localized states.

Figure 6 also shows that Δ_1 increases with w for very narrow nanoribbons and becomes almost independent of the GNR width for $w \gtrsim 10$. Other chiralities show a similar behavior (not shown here). These observations make it possible to relate our findings based on calculations for GNRs of $w \lesssim 20$ to experimentally realistic sizes, where

$w \approx 20 \dots 50$ ¹⁴.

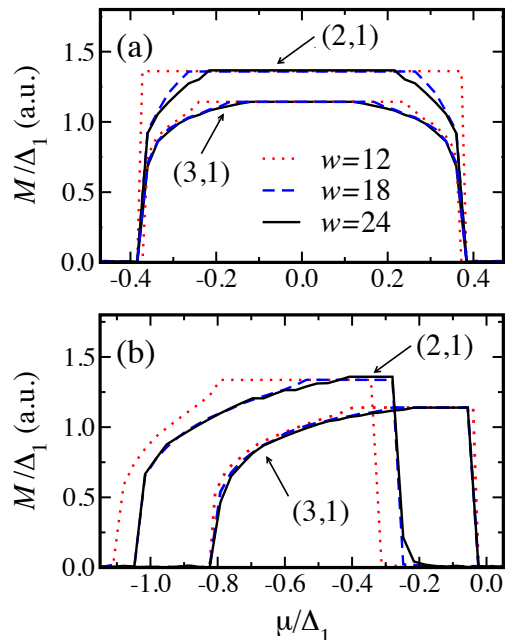


FIG. 7. (Color online) Edge magnetization M as a function of the chemical potential μ for chiral nanoribbons of different widths w for (a) $t'/t = 0.0$ and (b) $t'/t = 0.1$. In both cases $U/t = 1$.

We now turn to the analysis of the edge magnetization as a function of doping (or chemical potential μ). Figure 7 shows the magnetic moment per edge unit length M versus the chemical potential μ , scaled by Δ_1 . Here we use this $U/t = 1.0$. We find that, for sufficiently wide GNRs ($w \gtrsim 10$), the magnetization M/Δ_1 as a function of μ/Δ_1 becomes independent of w . This behavior is obtained for both the $t' = 0$ and the $t' \neq 0$ cases. Figure 7 indicates M is not a smooth function of μ . The reason is that the interedge antiferromagnetic phase is no longer the ground state of these GNRs away from half filling. The phase diagram is very rich, but M does not change appreciably. For this reason we did not pursue this line of investigation.

The chiralities we address above show a strong resemblance to GNRs with zigzag edges. We find that by increasing θ_c , for sufficiently wide GNRs, the edge magnetization M decreases almost linearly with θ_c and, as expected, vanishes for armchair terminations. The other limit is more interesting. For $U = 0$, by decreasing θ_c , one increases S and the degeneracy of the zero-energy states modes. For $U \neq 0$, these states split and give rise to a complicated band structure around half-filling as illustrated in Fig. 8(a) for the (8,1) chirality with $S = 7$, $P = 2$, and $I = 1$. The corresponding edge magnetization M as a function of μ is shown in Fig. 8(b). The latter clearly indicates that the nearly dispersionless modes of Fig. 8(a) are the ones that contribute most to M .

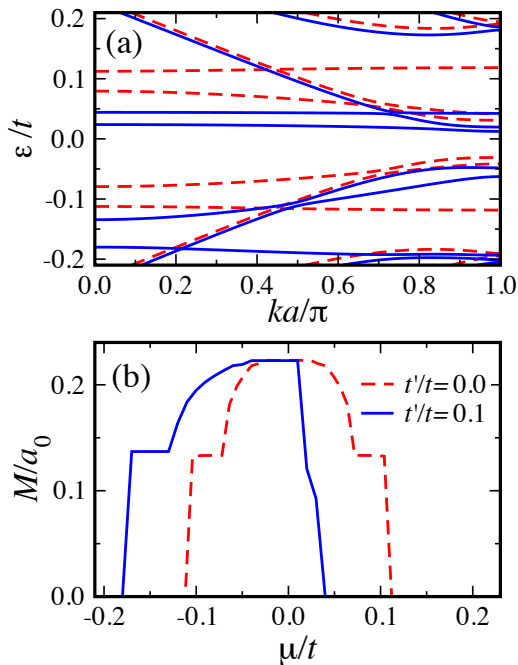


FIG. 8. (Color online) (a) Band structures of (8,1) chiral graphene nanoribbons of $w = 12$ and (b) edge magnetization M/a_0 as a function of the chemical potential μ/t . The dashed (red) lines stand for the case of $t'/t = 0.0$ and the solid (blue) ones stand for $t'/t = 0.1$.

C. LDOS in chiral graphene nanoribbons

As pointed out in the Introduction, the current experimental evidence for edge magnetization in GNRs is indirect: The local density of states measured by STS in graphene nanoribbons is claimed to show a behavior consistent with the theory for a variety of chiralities^{10,14}.

The STS data main features are the following¹⁴: When the tip is placed at the GNR edge the measured spectra display two clear peaks close the charge neutrality point. As the tip is moved away from the edge, the peak amplitudes are quickly suppressed. By moving the tip parallel to the edge, the peak amplitudes show modulations, with a period consistent with the size of the translation vector, $a = |\mathbf{C}_h|$ ¹⁴. In general, the peak heights show a large asymmetry that remains unexplained.

The experimental peak spacing has been associated with Δ_0 ^{10,14}. For that, it is necessary to take $U = 0.5t$, a value somewhat smaller than the conventional one²⁸, based on the argument of screening effects due to the metallic substrate. It is argued that the opening of an inelastic phonon scattering channel at $|\varepsilon| = 65$ meV makes it hard to observe higher energy peaks in the DOS. In what follows, we discuss how the nnn hopping term changes this picture.

In Fig. 9 we present the LDOS as a function of energy ε/t for a GNR of chirality (3,1). The LDOS is calculated along the edge (referred to as $y = 0$) and inside

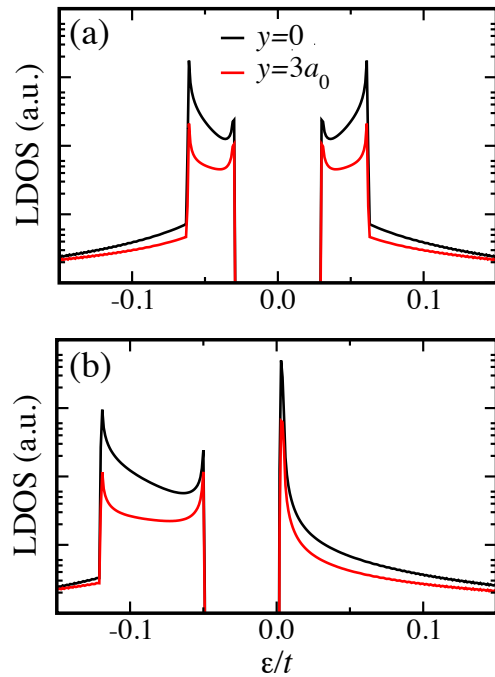


FIG. 9. (Color online) Local density of states for a (3,1) chiral graphene nanoribbon for (a) $t'/t = 0$ and (b) $t'/t = 0.1$. Here, $w = 12$ and $U/t = 1$.

the ribbon along the longitudinal orientation ($y = 3a_0$, in red). Figures 9(a) and 9(b) correspond to the $t'/t = 0$ and $t'/t = 0.1$ cases, respectively. We use $U = t$. The LDOS decreases exponentially with increasing y , indicating that the peaks in the LDOS correspond to edge states. Note that, for the realistic case of $t'/t = 0.1$, the LDOS peak amplitudes become asymmetric and the peak spacing can be understood in terms of Δ_0 and Δ_1 , defined in Figs. 5(c) and (d).

The GNR chirality (8,1) is experimentally analyzed in detail in Ref. 14 [see, for example, Fig. 2(c) therein]. Its corresponding low-energy band structure has a more complex one than that of the (3,1) case.

Figure 10 shows the LDOS of a GNR with chirality (8,1). From Fig. 8 we infer that the states that contribute most to the edge magnetization are those corresponding to the dispersionless bands. For $t' = 0$, the latter are located at $\varepsilon_1^a/t \approx \pm 0.08$ and $\varepsilon_1^b/t \approx \pm 0.12$. Accordingly, Fig. 10a shows that the LDOS peaks at the energies ε_1^a/t and ε_2^a/t are the ones that are most localized at the GNR edges. For the more realistic case of $t'/t = 0.1$, the states that predominantly drive the magnetization M (see Fig. 8b), are the flat bands at $\varepsilon_1^b/t \approx -0.18$, $\varepsilon_2^b/t \approx 0.02$, and $\varepsilon_3^b/t \approx 0.04$. The LDOS peak at $\varepsilon_4^b/t \approx -0.05$ corresponds to a van Hove singularity of an ordinary band, that is, a band whose states are not localized at the GNR edges. Hence, the band gap Δ_0 involves localized and delocalized states.

Let us now examine the local magnetization along the edges. In Fig. 11 we select values of ε/t corresponding to

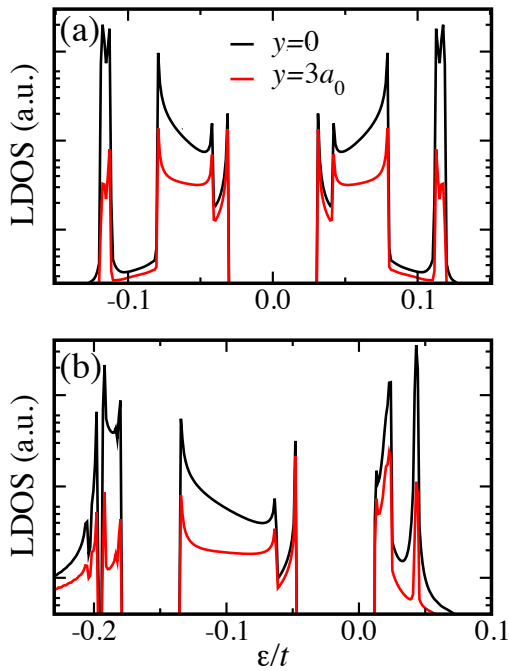


FIG. 10. (Color online) Local density of states of an (8,1) chiral graphene nanoribbon for (a) $t'/t = 0$ and (b) $t'/t = 0.1$. Here, $w = 12$ and $U/t = 1$.

the representative sharp peaks of Fig. 10 and plot the corresponding LDOS and edge magnetization M as a function x , the position oriented along the GNR edge. The case $t'/t = 0$ corresponds to Fig. 11(a) and $t'/t = 0.1$ corresponds to Fig. 11(b). These figures indicate that the edge magnetization M and LDOS corresponding to the dispersionless states at $\varepsilon/t = 0.11$ (for $t'/t = 0$) and $\varepsilon/t = 0.04$ (for $t'/t = 0.1$) display a very similar behavior to x . This observation gives further support to the discussion of the previous paragraph, corroborating the picture that, for $S \gg 1$, the split dispersionless states dominate the edge magnetization.

IV. CONCLUSIONS

We study the electronic band structure, the local density of states, and the edge magnetization of chiral graphene nanoribbons using a π -orbital Hubbard model in the mean-field approximation. We show that the inclusion of a next-nearest hopping term t' in the tight-binding Hamiltonian that is necessary for the realistic modeling of the electronic properties of GNRs changes its band structure significantly: While $t' \neq 0$ has little effect on the average magnitude of the edge magnetization at the charge neutrality point, the nnn hopping term largely modifies

the behavior of M as a function of doping. We believe that these observations call for more realistic analysis of the spin-wave excitations in GNRs^{40–42}.

The most notable effect of a t' is on the density of

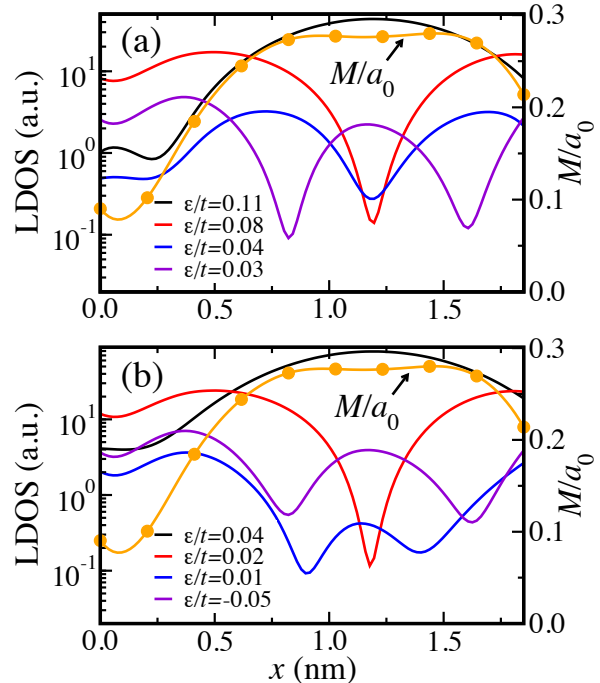


FIG. 11. (Color online) Local density of states (logarithmic scale) and edge magnetization (linear scale) M of an (8,1) chiral graphene nanoribbon for (a) $t'/t = 0$ and (b) $t'/t = 0.1$. Here, $w = 12$ and $U/t = 1$.

states. Our study indicates that the interpretation of STM/STS data is very different for $t' = 0$ and the more realistic case of $t'/t = 0.1$. In the latter and for the (8,1) chirality, the energy peak spacing $\delta = \varepsilon_3^b - \varepsilon_2^b$ and the peak height asymmetry are consistent with the results reported in Ref. 14. However, in analogy to the discussion of Δ_1 , we do not expect δ to depend on the width of the GNR w . We believe that an experimental LDOS study of the GNR for a fixed chirality and different widths can be of great help for the understanding of the edge magnetization in GNRs.

ACKNOWLEDGMENTS

We thank R. Capaz and E. Mucciolo for very helpful discussions. This work was supported by the Brazilian funding agencies FAPERJ, CAPES, CNPq, and INCT - Nanomateriais de Carbono.

¹ A. H. Castro Neto, N. M. R. Peres, K. S. Novoselov, A. K. Geim, and F. Guinea, *Rev. Mod. Phys.* **81**, 109 (2009).

² O. V. Yazyev, *Rep. Prog. Phys.* **73**, 056501 (2010).

- ³ K. Nakada, M. Fujita, G. Dresselhaus, and M. S. Dresselhaus, *Phys. Rev. B* **54**, 17954 (1996).
- ⁴ M. Fujita, K. Wakabayashi, K. Nakada, and K. Kusakabe, *J. Phys. Soc. Japan* **65**, 1920 (1996).
- ⁵ K. Kusakabe and M. Maruyama, *Phys. Rev. B* **67**, 092406 (2003).
- ⁶ J. Fernández-Rossier and J. J. Palacios, *Phys. Rev. Lett.* **99**, 177204 (2007).
- ⁷ Y.-W. Son, M. L. Cohen, and S. G. Louie, *Nature* **444**, 347 (2006).
- ⁸ L. Pisani, J. A. Chan, B. Montanari, and N. M. Harrison, *Phys. Rev. B* **75**, 064418 (2007).
- ⁹ J. Jung, T. Pereg-Barnea, and A. H. MacDonald, *Phys. Rev. Lett.* **102**, 227205 (2009).
- ¹⁰ O. V. Yazyev, R. B. Capaz, and S. G. Louie, *Phys. Rev. B* **84**, 115406 (2011).
- ¹¹ Z. Klusek, Z. Waqar, E. A. Denisov, T. N. Kompaniets, I. V. Makarenko, A. N. Titkov, and A. S. Bhatti, *Appl. Surf. Sci.* **161**, 508 (2000).
- ¹² Y. Kobayashi, K. I. Fukui, T. Enoki, K. Kusakabe, and Y. Kaburagi, *Phys. Rev. B* **71**, 193406 (2005).
- ¹³ K. A. Ritter and J. W. Lyding, *Nature Mater.* **8**, 235 (2009).
- ¹⁴ C. Tao, L. Jiao, O. V. Yazyev, Y.-C. Chen, J. Feng, X. Zhang, R. B. Capaz, J. M. Tour, A. Zettl, S. G. Louie, H. Dai, and M. F. Crommie, *Nature Phys.* **7**, 616 (2011).
- ¹⁵ Z. Chen, Y.-M. Lin, M. J. Rooks, and P. Avouris, *Physica E* **40**, 228 (2007).
- ¹⁶ M. Y. Han, B. Özyilmaz, Y. Zhang, and P. Kim, *Phys. Rev. Lett.* **98**, 206805 (2007).
- ¹⁷ M. Y. Han, J. C. Brant, and P. Kim, *Phys. Rev. Lett.* **104**, 056801 (2010).
- ¹⁸ E. R. Mucciolo, A. H. Castro Neto, and C. H. Lewenkopf, *Phys. Rev. B* **79**, 075407 (2009).
- ¹⁹ M. Wimmer, I. Adagideli, S. Berber, D. Tománek, and K. Richter, *Phys. Rev. Lett.* **100**, 177207 (2008).
- ²⁰ X. Li, X. Wang, L. Zhang, S. Lee, and H. Dai, *Science* **319**, 1229 (2008).
- ²¹ L. Jiao, X. Wang, G. Diankov, H. Wang, and H. Dai, *Nature Nanotech.* **5**, 321 (2010).
- ²² D. V. Kosynkin, A. L. Higginbotham, A. Sinitskii, J. R. Lomeda, A. Dimiev, B. K. Price, and J. M. Tour, *Nature* **458**, 872 (2009).
- ²³ A. R. Akhmerov and C. W. J. Beenakker, *Phys. Rev. B* **77**, 085423 (2008).
- ²⁴ L. Sun, P. Wei, J. Wei, S. Sanvito, and S. Hou, *J. Phys.: Condens. Matter* **23**, 425301 (2011).
- ²⁵ K. Wakabayashi and S. Dutta, *Solid State Communications* **152**, 1420 (2012).
- ²⁶ W. Jaskólski, A. Ayuela, M. Pelc, H. Santos, and L. Chico, *Phys. Rev. B* **83**, 235424 (2011).
- ²⁷ Y.-W. Son, M. L. Cohen, and S. G. Louie, *Phys. Rev. Lett.* **97**, 216803 (2006).
- ²⁸ Y. Hancock, A. Uppstu, K. Saloriotta, A. Harju, and M. J. Puska, *Phys. Rev. B* **81**, 245402 (2010).
- ²⁹ S. Dutta, S. Lakshmi, and S. K. Pati, *Phys. Rev. B* **77**, 073412 (2008).
- ³⁰ S. Dutta and K. Wakabayashi, *Sci. Rep.* **2**, 519 (2012).
- ³¹ H. Feldner, Z. Y. Meng, A. Honecker, D. Cabra, S. Wessel, and F. F. Assaad, *Phys. Rev. B* **81**, 115416 (2010).
- ³² M. Golor, C. Koop, T. C. Lang, S. Wessel, and M. J. Schmidt, *Phys. Rev. Lett.* **111**, 085504 (2013).
- ³³ M. Golor, T. C. Lang, and S. Wessel, *Phys. Rev. B* **87**, 155441 (2013).
- ³⁴ M. Schüler, M. Rösner, T. O. Wehling, A. I. Lichtenstein, and M. I. Katsnelson, *Phys. Rev. Lett.* **111**, 036601 (2013).
- ³⁵ J. Jung and A. H. MacDonald, *Phys. Rev. B* **87**, 195450 (2013).
- ³⁶ P. Koskinen, S. Malola, and H. Häkkinen, *Phys. Rev. Lett.* **101**, 115502 (2008).
- ³⁷ E. H. Lieb, *Phys. Rev. Lett.* **62**, 1201 (1989).
- ³⁸ J. Jung and A. H. MacDonald, *Phys. Rev. B* **79**, 235433 (2009).
- ³⁹ K. Sawada, F. Ishii, M. Saito, S. Okada, and T. Kawai, *Nano Lett.* **9**, 269 (2009).
- ⁴⁰ K. Wakabayashi, M. Fujita, H. Ajiki, and M. Sigrist, *Phys. Rev. B* **59**, 8271 (1999).
- ⁴¹ O. V. Yazyev and M. I. Katsnelson, *Phys. Rev. Lett.* **100**, 047209 (2008).
- ⁴² F. J. Culchac, A. Latgé, and A. T. Costa, *New J. Phys.* **13**, 033028 (2011).